JNC TN9400 2001−115

Interpretation of the CABRI LTX Test using the SAS4A Code

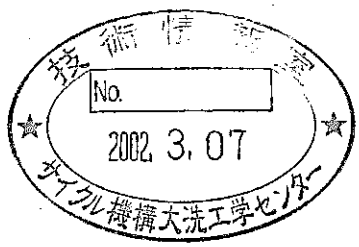

October, 2001

O-arai Engineering Center
Japan Nuclear Cycle Development Institute

Ⓚ

Interpretation of the CABRI LTX Test Using SAS4A-Code

Soo-Dong SUK[*1] and Ikken SATO[*2]

Abstract

The LTX test was performed using a SCARABIX pin in March 2000 in the framework of the CABRI RAFT Program to investigate the pin failure mechanism, in-pin fuel motion and post-failure fuel relocation behavior under a simulated TUCOP accident in LMFR. The transient of the test was initiated by a coolant flow reduction and a structured TOP was triggered when coolant average temperature at TFC reached a predefined value to keep the channel in the subcooled condition. Pin failure occurred rather early, before the initiation of any significant fuel melting. This early failure of the cladding was presumably caused by a local cladding heatup and stress concentration arising from the excessive pin bending. Rapid gas release upon the cladding failure led to the voiding of coolant channel, followed by a molten fuel ejection and gradual axial relocation in the test channel.

An effort was made to interpret the experimental results of the LTX test using the SAS4A code. Although the original SAS4A model was not well fitted for this type of early pin failure, the global behavior after the pin failure was reasonably simulated with time and axial location of the pin failure specified as an input to the code and judicious choice of failure criteria. This study resulted in better understanding on the gas release behavior from the failed fuel pin and its effect on the process of the post-failure fuel melt progression and relocation. It appears that the detail mechanism of the early cladding failure does not affect the global behavior of the post-failure fuel melt progression and relocation.

---

*1: KALIMER Development Team, Korea Atomic Energy Research Institute

*2: Advanced Technology Division, O-arai Engineering Center, JNC.

SAS4A コード解析による CABRI LTX 試験評価

（研究報告）

Soo-Dong SUK[※1]　　佐藤　一憲[※2]

要旨

CABRI-RAFT 計画の LTX 試験は、SCARABIX 燃料を用い高速炉の TUCOP（Transient Under-Cooling Over-Power）型過渡条件下における燃料ピンの破損メカニズム、ピン内燃料移動、及び破損後燃料移動挙動を解明することを目的として、2000 年 3 月に実施された。本試験における過渡は、冷却材流量減少によって開始し、フィッサイル頂部における冷却材平均温度が、サブクール度を保つべく予め設定された条件に達した時点で過出力が印加された。本試験では、燃料溶融に至る前の早期の燃料ピン破損が生じた。この早期の被覆管破損は多分に顕著なピン湾曲に起因した局所的な高温化によるものと考えられる。被覆管の破損によってピン内からの急速なガス放出が生じ、冷却材流路のボイド化を生じた。その後、溶融燃料の放出が生じ、徐々に冷却材流路中での軸方向移動を生じた。

本研究では、SAS4A コードを用いた解析により LTX 試験の解釈を行った。もともとの SAS4A コードはこのような早期破損条件に適合したものではないが、被覆管の破損時間と位置を入力条件によって指定するとともに、溶融燃料放出や燃料崩壊について適切な判定条件を選定することで、破損後の全般的な挙動を妥当に模擬できた。本評価によってガス放出挙動がより明確に把握でき、その燃料溶融拡大や燃料移動への影響をも良く理解することができた。

なお、本試験における早期破損メカニズムそのものは実機における代表性を有するものではないと考えられるが、早期破損を境界条件とした場合のその後の燃料溶融拡大や燃料移動挙動については実機評価に有効なデータである。

※1 韓国原子力研究所　KALIMER 開発チーム（原子力交流制度に基づく研究者としてサイクル機構内にて本研究を実施）

※2 大洗工学センター　要素技術開発部　リスク評価研究グループ

TABLE OF CONTENTS

LIST OF TABLES

Page

LIST OF FIGURES

1. Introduction

The LTX test was performed in March 2000 as part of the CABRI RAFT Program. The objectives of the test were to investigate the pin failure mechanism, in-pin fuel motion and post-failure fuel relocation behavior under a TUCOP(Transient Undercooling Overpower) in sodium coolant channel. The test conditions are essentially the same as those of the preceding LT4 test [1], which had been carried out in March 1997 in the framework of the CABRI FAST program. A SCARABIX pin, a mixed-oxide annular fuel with a maximum burnup of 6.4 at.%, was used in semi-restrained channel conditions for each of the tests. Modifications were made for the LTX test by replacing solid fertile pellets by hollow insulation pellets and placing DT (Displacement Transducer) to detect in-pin fuel squirting, which was suspected to have occurred in the LT4 test.

Linear heat rate at the peak node of the pin and sodium temperature rise along the fissile were 507 W/cm and 180°C, respectively, during the CABRI steady-state. The transient was initiated by a coolant flow reduction from the steady-state value of 135 g/s(571 l/h) with a halving time of about 7 seconds. A structured TOP was triggered at 18.5 sec after the initiation of LOF when coolant average temperature at the fissile top reached a predefined value to keep the channel in the subcooled condition. Extensive azimuthal temperature oscillations were observed during the LOF and a local onset of sodium boiling took place during the pre-pulse period of the TOP.

Quite contrary to what happened in the LT4 test, i.e., pin failure occurred late with extensive fuel melting, a cladding failure occurred rather early at around 460 ms after TOP, before any initiation of significant fuel melting or sodium boiling. An analysis[2] of the LTX test using the PAPAS-2S code shows that the earlier cladding failure could be due mainly to local cladding heat-up caused by excessive pin bending occurred in the LTX test. Upon the cladding failure, a rapid gas release led to an extensive coolant-channel voiding. Under the circumstances, the continued power transient in the test gave rise to progressive fuel melting and subsequent axial relocation of molten fuel similar to the other CABRI TUCOP tests with extended coolant boiling conditions. Because of limited energy injection, fuel disruption and axial relocation were finally contained within the fissile region. A significant blockage of the test channel appeared after the transient, with a flow rate reduced to 3 % of the

initial flow.

In this study, the SAS4A code, version "REF99 Release 3, is utilized to simulate the sequence of events through the transients of LOF and TOP as well as the pre-irradiation history and steady state power operation. The focus is made, however, on demonstrating the limitations as well as the ability of the code to predict the post-failure fuel behavior in the TUCOP test like the LTX.

2. Major Test Features and Results

2.1 Test Features

A structured TOP was automatically triggered when the mean sodium temperature at TFC reached 893 °C with sodium flow rate decreased to 40 g/s (168 l/h). Figure 2.1 shows the power history during the TOP. At the end of pre-pulse (480 ms after the TOP onset), energy release at the peak power node (PPN) was increased to 0.49 kJ/g. Its value reached up to 1.11 kJ/g at the time of scram (720 ms), and saturated to 1.23 kJ/g by the end of the TOP(1.2 s). Transient power increased by 45.4 times the steady-state power at 543 ms after the onset of TOP.

A SCARABIX pin was used in the LTX test as in the LT4 test. The pin is a mixed-oxide annular fuel pellets of 21.4% Pu /U+Pu pre-irradiated in PHENIX to a local burnup of 6.4 at.%, clad in 15/15 Ti with an outer radius of 8.5 mm. For the LTX test, modifications were made on the test pin used in the LT4 test by replacing original solid fertile pellets by hollow insulation pellets to study in-pin fuel motion expected to take place during the test, particularly the fuel squirting before cladding failure toward the gas plena through the central holes connecting the fissile region and gas plena. A new device was installed just above TFC to detect the squirted fuel moving upward from the fissile. Table 2.1 lists the test features of interest for the two tests.

2.2 Test Results

During LOF of the test, the elongation of fissile fuel of 2 ($\pm$2) mm was observed by the neutron hodoscope, while it was 3($\pm$2) mm in the LT4 test. Although relatively large uncertainty in the measurements makes a direct comparison of the fuel elongation difficult, the slight difference is consistent with more extensive pin

bending expected in the LTX test than in the LT4 test. The azimuthal coolant temperature variation at TFC was 39.7 K at the end of the LOF in the LTX test and increased further during TOP of the test. It was 33.9 K at the end of LOF in the LT4 test. The azimuthal temperature difference at 60cm BFC (Bottom of Fissile Column) was also larger than in the LT4 test. Furthermore, the peak coolant temperature took place at about 60 cm BFC, as indicated by TC75 (280 °), during TOP of the LTX test, while it was around TFC in the LT4 test.

Figure 2.2 shows sodium flow rates during TOP. Local sodium boiling began at around 410 ms after TOP during the pre-pulse in 60cm BFC, leading to a moderate sodium expulsion from the channel. A more violent sodium expulsion transient took place at 460 ms, before onset of the main pulse, apparently caused by the cladding failure and subsequent gas release. Unfortunately, some important instrumentation malfunctions took place during the test. Due to some unsuitable configuration as well as connectivity problems, the microphone and the pressure measurements failed. As a result, precision was lost for the timing of the rupture events and their locations.

Various events of measurement are shown along with the flowmeter integral curve in Figure 2.3. After the peak of the main pulse (560 – 670 ms), the progressive destruction of the TCs in the test channel near the presumed rupture location (on the levels of 30, 45, 60 cm BFC) indicated the fuel ejection. In the mean time, the DT caught a dynamic event at 526 ms. About 4 ms later, the hodoscope registered a signal increase at TFC. However, the PTE did not reveal any sign of in-pin molten fuel relocation above TFC. The DT event and subsequent hodoscope event are considered, therefore, to have been upward motion of the upper part of the pin. The squirting detection device was also found in the original unreleased state. There were no correlated TC events at TFC.

Based on the PTE results, the DT event and subsequent hodoscope event are considered to have been upward motion of the upper part of the pin, taking place at 526 ms. Figure 2.4 illustrates final state of the test fuel deduced from the hodoscope data. The results show the trend of the fuel accumulation around TFC and in the upper zone from row 12 to 20(55 to 73 cm above BFC), noticeable lack of fuels in the mid-zone from row 21 to 32(30 to 55 cm from BFC), and accumulation in rows 41 to 44(6 to 15 cm from BFC). Results of the post-test non-destructive examinations by gammametry and X-ray images are in general agreement with the trend described in

the above. It was also shown that the clad had been severely damaged and not visible between 31.3 and 59.6 cm BFC, the pin nose had been displaced in the upward direction by 17 mm. No molten fuel was observed in the central hole above or around TFC.

Within the PTE activity for the LTX test, an axial cut covering from 76.0 to 79.5 cm BFC was performed to provide detail information of the pin behavior at around TFC, including the level of the intact cladding, upper steel accumulation, the failure mode of the brasing, among others. It was observed in the examination that steel cladding was intact down to about 76.9 cm BFC, molten steel accumulated between 77.3 and 76.0 cm BFC, small amount of fuel accumulated above the accumulated steel, and few fuel fragments existed above TFC.

3. Analysis Assumptions and Bases

3.1 Failure Specifications and Criteria

There are three major events of fuel pin failure in simulating the molten fuel behavior using the SAS4A code. They include cladding failure and gas release, pin failure (fuel melting causing cladding rip-off or separation), and fuel disruption, which take place simultaneously or in sequence depending on the specific transient. Since the major interest of this study is the molten fuel behavior after clad failure, the time and axial locations of the clad failure were specified as inputs to the code in this study, based on the interpretation of the test data.

First, it is assumed for the analysis that clad failure occurred at around 60 cm above BFC at 460 ms after the onset of TOP. The test data, shown in Figure 2.2, indicates time of the clad failure as evidenced by a rapid flow-rate divergence. There seems to be no direct measurement to indicate where it failed in the test, however. As described in Section 2, the peak sodium temperature occurred at 60cm BFC rather than at TFC seemingly because of an excessive pin bending occurred in the test. It is deduced from the experimental data and analysis with PAPAS-2S that the cladding mid-wall temperature at the hottest TC azimuth of 60cm BFC reaches beyond 1050 °C by the time of 460 ms after the TOP onset. At this temperature level, the cladding hoop stress corresponding to the plenum gas pressure could be enough to induce cladding failure.

Secondly, it is basically assumed in the analysis that the molten fuel ejection occurs at 526 ms upon the onset of TOP at 60cm BFC, the axial location of cladding failure. As presented in Section 4.3, this assumption was not directly realized in the SAS4A analysis because of the model limitation. At this time, a significant upward displacement of the pin top took place. However, there was no evidence of corresponding upward relocation of the fissile bottom. This clearly indicates that the pin was separated into the upper and lower parts. Although there was no direct information on the axial level of such a separation, pin failure is most likely to have occurred at 60 cm BFC judging from the temperature history. It is assumed, therefore, that the test pin fails at the same axial location as the initial cladding failure. The high thermal load at this axial location expected from Niobium structure also supports the above assumption, since this indicates the accumulation of the molten fuel. Based on the DT signal at 526 ms/ TOP and subsequent hodoscope event, and the PTE results as well, the following sequence of events are assumed to have occurred around the time of pin failure ; Fuel pin separation takes place at 526 ms by losing the strength at the axial location of around 60 cm BFC, where the upper edge of melt front of the fuel is reaching at the time of failure. The upper pin separated from the lower one moves upward into the free space above the pin and stays there during the test.

Finally, fuel disruption is expected under a rapid cladding heat-up and fuel melting after the fuel ejection. Criteria for fuel disruption are 20 % AMF(fuel areal melt fraction) and cladding midwall temperature of 1250°C as used in the previous studies with SAS4A. It should be noted that this cladding-temperature level is usually reached just after cladding dryout in the conventional situations.

3.2 Plenum-Gas Blowout Model

In the SAS4A model, failure prediction is linked to the ejection of molten fuel and its interaction with sodium and coolant-channel structures. For the condition of single-phase coolant , therefore, cladding failure is allowed only after some amount of fuel melting gets available. Under the circumstances, the plenum-gas blowout model, usually applied after coolant boiling, had been used for simulating early cladding failure and subsequent gas release in the studies with the SAS4A code. In order to simulate the LTX test, some modifications were necessary to correct the

inconsistency handling the condensation of gas mixture between the pre- and post-failure models. Input parameters specifically selected in this study are listed in Table 2.2. These inputs are essentially same as those used in the SAS4A analysis of the LT1 study [3] for the condition of single-phase coolant

4. Analysis Results

4.1 Pre-Failure Analysis

Figures 4.1, 4.2 and 4.3 show a set of major input variables of SAS4A being compared with the test conditions, which include power history normalized to the steady-state power, axial power distribution during the steady state and flow rate during LOF. It can be seen that the basic features of the test are well fitted for the analysis. It is also shown in Figure 4.4 that the steady-state coolant temperature distribution is well simulated along the channel with the code. Figure 4.5 shows a comparison of the coolant temperature history at TFC during LOF between the TC data and the analysis result by the code. It can be noticed that there exist variations of the TC signals presumably because of pin bending, which is not modeled in the SAS4A code. Pin bending appears to cause the trend of a slight underestimation of the coolant temperature by the code.

Figures 4.6 and 4.7 present comparison of coolant temperature histories measured by TCs at various azimuthal angles with the analysis results at TFC, and 60 cm above BFC , respectively, during the early phase of the TOP. As can be seen in the figures that the coolant heat-up behavior is well simulated by the code during TOP up to the time of cladding failure. It may be noted in Figure 4.6 that the calculated coolant temperature at TFC temporarily decreases from 940 °C at 526 ms upon the onset of TOP as much as 40 °C just prior to the step increase up to 1270 °C. On the other hand, the coolant temperatures measured by TCs slowly increases toward the saturation temperature. As described in the analysis report of the LT1 test[3], a sudden dip of the temperature arises from the upward motion of the relatively cold coolant slug from down below. The absence of coolant temperature drop in the experiment is partially explained with the possible delay of TC response on one hand. On the other hand, axial temperature profile in the experiment may have been flatter than in the calculation. As the slug passes through TFC, the coolant channel

subsequently becomes filled with the released gas (in about 20 ms). However, heat transfer between the ejected gas and channel structure cannot be modeled under the present usage of the SAS4A code. This results in a sudden step increase of the coolant temperature to the peak in the analysis work. The insufficient modeling for the possible heating of the coolant-channel structure by the gas released in this study would not affect the results, however, because heating of the cladding after channel voiding will be dominated by the heat flow from internal fuel pellets and/or molten fuel in the coolant channel.

4.2 Cladding Failure and Gas Blowout Analysis

Figures 4.8 and 4.9 show the axial cladding temperature distribution and radial fuel temperature profile at PPN, respectively, calculated at the time of the cladding failure (460 ms after the TOP onset). Cladding temperature reaches about 1000 °C at the location of failure and fuel temperature remains far below the melting point at the time of the cladding failure and subsequent gas blowout.

Figure 4.10 presents analysis results by SAS4A and test data for coolant flow rates in the outlet as well as in the inlet of the test channel around the time of the cladding failure and gas release. It can be seen that the overall trend of flow divergence, that is the magnitude and duration of the flow rates, is well simulated by the code. It may be noted herein that a failure rip area of $1mm^2$ was used in this analysis, as specified in Table 2.2. This rip area is lower than the value($3\ mm^2$) used in the LT1 test representation[3]. Right upon the cladding failure and initial gas blowout at 460ms after the onset of TOP, calculated flow rates increase to the peak values in step and subsequently in gradual decline. The pin fails at around 529 ms in the analysis and the flow rates show local peaks and then continue to decrease. As the lower void front reaches the lower boundary of the channel set by the code at about 590 ms, flow stops at the inlet of the channel. The upper void front subsequently hitting the upper boundary at 680 ms or so, flow stops after a brief peak at the outlet of the channel. Void fronts, which are the integration of the flow rates, are compared in Figure 4.11. It can be seen that the initial rate of void development is well simulated but void fronts are delayed a bit (about 40 ms or so) in the analysis compared to what happened in the test. This may well be caused by the lack of modeling for the onset of local boiling, which appeared to have occurred in the test at 420 ms after TOP. A

sudden cease of the void-front expansion is due to the limit set by the code itself for the sake of computational stability.

4.3. Pin Failure and Melt Progression Behavior

Figures 4.12 and 4.13 illustrate the axial distribution of cladding mid-wall temperature and the melting boundary, respectively, calculated at 529 ms after the triggering of TOP. The cladding temperature reached about 1100 °C at around the failure location by this time. Fuel melting was initiated at 45 cm above BFC (core node 14) at around 500 ms after TOP. By the time of the pin failure, significant fuel melting had occurred and the axial melt front expanded from 28 cm to 56 cm above BFC. The areal melt fraction is peaked at 14 % around 45 cm BFC. Fractional radii of the melting boundary ranged from 80 to 90 %. In Figure 4.13, it can be noted that fuel remains solid in the inner region while molten in outer region of the fuel pin. This represents a radial temperature inversion characteristic with the CABRI test.

As described in Section 3.1, the test results are interpreted such that molten fuel ejection took place at 60 cm above BFC at 526 ms after TOP. One of the failure criteria is that some fraction of melting should take place. In our analysis, however, melt front reaches 60 cm BFC only after about 10 ms later than the interpreted time of failure in the test. Thus it was arranged in the analysis that fuel pin fails upon the melt front reaching at 56cm BFC, a node below the failure node, to put the time of failure forward close to 526 ms.

Early phase of melt progression is schematically depicted up to the time of peak power (545 ms after TOP) in Figure 4.14. At about 500 ms after TOP, fuel melting is initiated at the peak power node (about 45 cm above BFC, channel node 18). Upon the pin failure at 529 ms after TOP, molten fuel is ejected from the failure node of the pin to the voided channel. The liquid sodium stays just below BFC and far above TFC at the time of fuel ejection into the channel so that no significant fuel-coolant interaction is anticipated in this kind of TUCOP event. Prior to the power peaks at 545 ms/TOP, only a small amount of mixture of the chunk, crust and melt of the fuel is formed around the cladding as well as the structure at the same axial level as the failure node. As can be seen in Figure 2.1, the energy release amounted to 0.75 kJ/g or 60 % of the total energy release by this time.

Right after the peak power (at 549 ms/TOP), the first fuel disruption occurs at

the location of the pin failure and propagates rapidly downward along the pin. This may be well illustrated in Figure 4.11, which shows axial propagation of fuel disruption together with the development of the void-fronts in the channel. As can be seen, fuel disrupts extensively by 650 ms, which corresponds to the time of the end of the main power pulse with energy release reaching more than 1.0 kJ/g (80 % of the total energy). By this time, fuel disruption has propagated down to 25 cm and up to 65 cm above BFC. Fuel disruption is taking place gradually to the limited extent afterward. It is probable that the earlier TC rupture events below the failure location are more related to the ejection of molten fuel. It may be noted in the figure that the fuel disruption fronts calculated by the code reasonably well reflect a series of the events of TC rupture.

Figure 4.15 presents the melt progression phenomena including fuel disruption and relocation, from after the power peak down prior to the reactor scram at 720 ms/TOP, by which time 1.11 kJ/g of energy (90 % of total energy release) have been injected to the pin. When the initial fuel disruption occurs at the channel node 21(core node 17) at 549 ms/TOP, some amount of molten fuel and crust are formed around the structure of the channel but it is mostly chunk fuel blocking the channel. As fuel disruption progresses downward, molten fuel in the central locations down below moves upward in the pin and is ejected through the upper node into the channel and stay upward in the channel, before the central nodes disrupt for themselves at around 590 ms/TOP. As fuel disruption continues, the epicenter of the ejected fuel also moves downward. It may be noted that the void front reached the lower limit and upper limit at around 590 ms and 680 ms/TOP, as described earlier. In the mean time, the plenum gas continues to be released from lower and upper ends of the pin even after the initial blowout upon cladding failure. This tends to drive the fuel and steel ejected to the either end of the fissile region.

Final phase of the melt progression and relocation is illustrated in Figure 4.16. The fuel pin gradually disrupts to the extent that only about 10 cm-long stubs from either end of the pin stay intact. The mixture of the fuel and steel is gradually relocated to the ends of the pin due to the continual release of plenum gas and gravity effect as well. Since the energy release is saturated after the scram, the relocation of the mixture of the fuel and steel tend to be limited within fissile. However, the molten steel gets relocated upward to the above of TFC. This result is consistent with a result of

the PTE performing the axial cutting of the zone around TFC. However, a small amount of fuel accumulated above the molten steel as well as a few fuel fragments above TFC observed in the PTE are not predicted by the code. These are not considered local effects significant enough to be simulated by the code, in which the main part of the event sequence is represented. Unfortunately, processing of the hodoscope data is still underway to deduce the transient fuel mass distribution so that no quantitative result is available at present.

Figure 4.17 presents a comparison of the final fuel configuration calculated by the SAS4A code to that deduced from the preliminary hodoscope data (See Figure 2.4). It should be reminded that the hodoscope signal is not proportional to fuel mass due mainly to the self shielding effect. Therefore one should only compare the trend of axial fuel distribution. It can be seen in the figure that the code predicts rather well global behavior of the test data; the fuel accumulation around TFC and in the upper zone of the channel above 55 cm BFC, sharp drop of fuel at around 50 cm BFC, gradual accumulation of fuels in the central part of the core down to 30 cm BFC, and accumulation of fuel below at about 15 cm BFC. It may be noted, however, that there exist a few local deviations between the test data and the calculated results. It should be noted that the test data only shows the fuel mass increased from the steady state value. Above TFC, for instance, a small amount of increase in fuel mass would give rise to a large signal. A peak at around TFC appears to be arising from the fuel elongation occurred during TOP as well as LOF or insignificant amount of molten fuel relocation. Another peak is shown at about 35 cm BFC in the hodoscope data, while the code predicts gradual increase of fuel mass downward. Judging from the experience with the code, this appears to represent the tendency of the code to underpredict the downward fuel relocation.

The trend of fuel relocation in the channel as well as in-pin melt progression described in the above may be better understood by looking into the relative fuel-worth history during TOP, which is shown in Figure 4.18. The relative fuel worth used herein is defined considering the fuel mass distribution and axial power profile in CABRI. The initial value is unity and the relocation of fuel mass from the higher power region to the axial ends of the fissile leads to the reduction of the relative worth. It can be seen that the relative worth drops upon pin failure at 529ms/TOP as molten fuel of the central part of the pin, where the worth is higher, moves upward in the pin

and ejected through the upper part of the pin. It is likely that downward propagation of the fuel disruption leads to disappearance of the "pipe" which has been serving as an important means to transfer the fuel up to the high axial level, where the power is low. From around 600 ms on, the relative worth increases as the molten fuel from the lower part of the pin (as low as 25 cm BFC) is ejected through the central location. As described above, the downward movement of the epicenter of the ejected fuel toward the central location of the channel would also contribute to this trend of worth increase. After 680 ms or so, the fuel worth continues to decrease as the epicenter of the ejected fuel moves down away from the central nodes. As described in the above, the fission gas continually released from the plena tends to disperse the fuels to the ends of the fissile region, which contributes to the decrease of the relative fuel worth.

5. Conclusion

An effort has been made to simulate the experimental results of the LTX test using the SAS4A code. In the test, the pin cladding failed rather early before the initiation of any significant fuel melting, presumably due to fuel pin bending. Given the time and axial location of the cladding failure and fuel ejection, the code produced the results quite consistent with the experimental results including the fuel disruption and melt progression behavior as well as the coolant channel voiding and subsequent heat-up of the pin. This study vindicates conclusions drawn up in the LT1 analysis [3] in terms of the ability of the code to predict the early- induced events and validity of the present treatment for dependency of the mobility of disrupted fuels on fuel enthalpy, even if the initial pin boundary conditions are quite different between the two tests.

There currently exists quite a limited amount of experimental data for the LTX test. Precision was also lost for the timing of the rupture events and their locations. For the analysis of the test, therefore, it was necessary to assume the major events by interpreting indirect information from the test. One of the major assumptions or interpretations made for this analysis is related to the specification (time, location and mechanism) of the molten fuel ejection; molten fuel starts to get ejected upon the axial separation of the cladding at around 60 cm BFC (location of the cladding failure) at 526 ms after the onset of TOP. The application of this interpretation gave rise to a simulation quite close to the experimental results of post-failure fuel behavior. The

successful simulation by the SAS4A code of global behavior of the post-failure molten fuel behavior in the LTX test confirms the observation made in the previous study in that the code may well provide a sound basis for future evaluation of the early failure scenario in the reactor case, regardless of the details of the cladding failure.

Acknowledgement

This study has been made as part of the MEXT Scientist Exchange Program of Japan ~~and~~ National Long-Term Nuclear Energy Research Program of Korea. The authors express their great appreciation for Mr. Katsuhiko TAKAHASHI of Nuclear Engineering System Inc.,and Mr. Takuhiro CHUBACHI of CSK INC. , who helped the analytical works and preparation of the figures.

References

[1] Y. ONODA and I. SATO, "Interpretation of the CABRI LT4 test with SAS4A-code analysis," JNC TN9400 2001-047, March 2001

[2] Y. FUKANO and I. SATO, "Interpretation of the CABRI-RAFT LTX test up to pin failure based on detailed data evaluation and PAPAS-2S code analysis," JNC TN9400 2001-096, September 2001

[3] I. SATO and Y. ONODA, "Interpretation of the CABRI LT1 test with SAS4A-code analysis, " JNC TN9400 2001-048, March 2001

JNC TN9400 2001-115

"Interpretation of the CABRI LTX Test using SAS4A Code"

12 ページ（Acknowledgement）

誤：

This study has been made as part of the MEXT Scientist Exchange Program of Japan and National Long-Term Nuclear Energy Research Program of Korea.

正：

This study has been made as part of the MEXT Scientist Exchange Program of Japan which contributed to the National Long-Term Nuclear Energy Research program of Korea in the year of 2001.

Table 2.1 Comparison of test condition and main test results between the LTX and LT4 tests

	LTX	LT4
Fuel Type	Scarabix-CABRI	Scarabix-CABRI
Fissile length (mm)	750	750
Pin diameter (mm)	8.5	8.5
Po (W/cm)	507	512
Na Temp. at BFC (℃)	400	401
Na Temp. at TFC (℃)	580	579
Energy at end of pre-pulse(480ms) (J/g)	499	499
Energy at 720ms (kJ/g)	1.10	1.10
Energy at 1.2s (kJ/g)	1.22	1.22
TOP Trigger (s after LOF onset)	18.457	18.651
TFC Na Temp. at TOP onset (℃)	893	897
Boiling onset (ms after TOP onset)	407	398
Pin failure (ms after TOP onset)	460	621

Table 2.2 SAS4A input parameters selected for the analysis

Objectives	Variable name	Input location	Specified value	Usual value	explanation
Control plenum gas blowout behavior	IGASRL	(51, 278)	4	-	Select the option to specify the gas blowout time
	INDFAL	(51, 283)	17	-	Node number of gas blowout location
	AGSRLS	(64, 181)	1.0E-6	-	Rip area (m2)
	GASKOR	(64, 182)	3.0	-	Orifice coefficient for gas release from the plenum
	TMFAIL(1-30)	(64, 186 – 188)	2518.96	-	Gas blowout time (sec in SAS4A time)
Avoid liquid coolant slug disappearance	XKORV(1, 2)	(64, 56)	6.4	1.6	Orifice coefficient for flowing sodium at the inlet
Suppress condensation and evaporation in LEVITATE	CFNACN	(13, 1146)	0.0	6.3E4	Sodium condensation heat transfer coefficient
	CFNAEV	(13, 1147)	1.0E-6	6.0E5	Sodium evaporation heat transfer coefficient
Control initial liquid film	WFS00	(64,77)	1.0E-5	1.19E-4	Initial film thickness on the structure (m)
	WF0	(64, 84)	1.0E-5	1.19E-4	Initial film thickness on the cladding (m)
Prevent unrealistic dryout judgement	WFMNSW	(64,76)	0.67E-5	6.0E-5	Dryout film thickness on the structure (m)
	WFMNWT	(64, 75)	0.67E-5	6.0E-5	Dryout film thickness on the cladding (m)

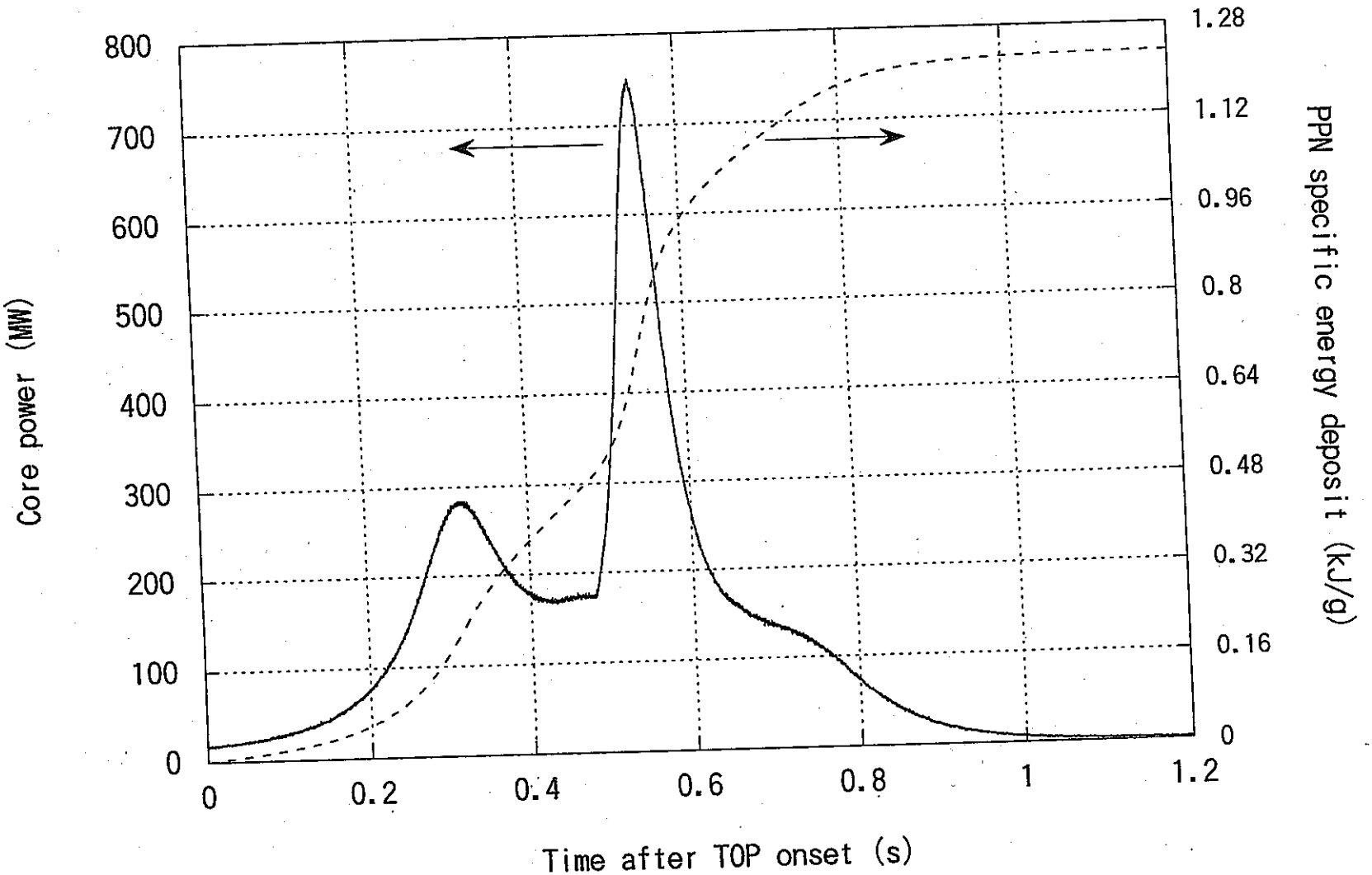

Figure 2.1 **Power and energy release history during TOP**

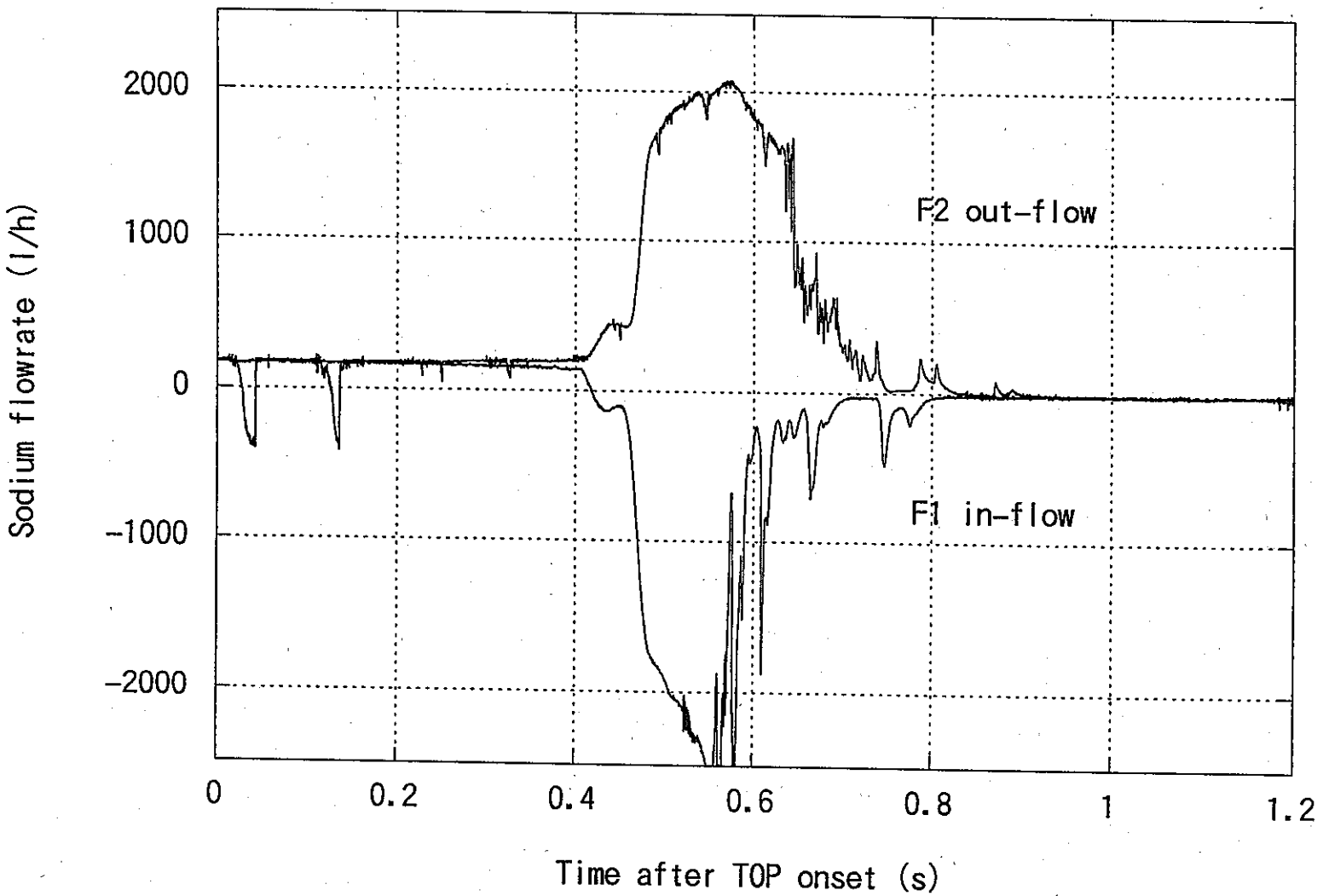

Figure 2.2 **Coolant flow rate response during TOP**

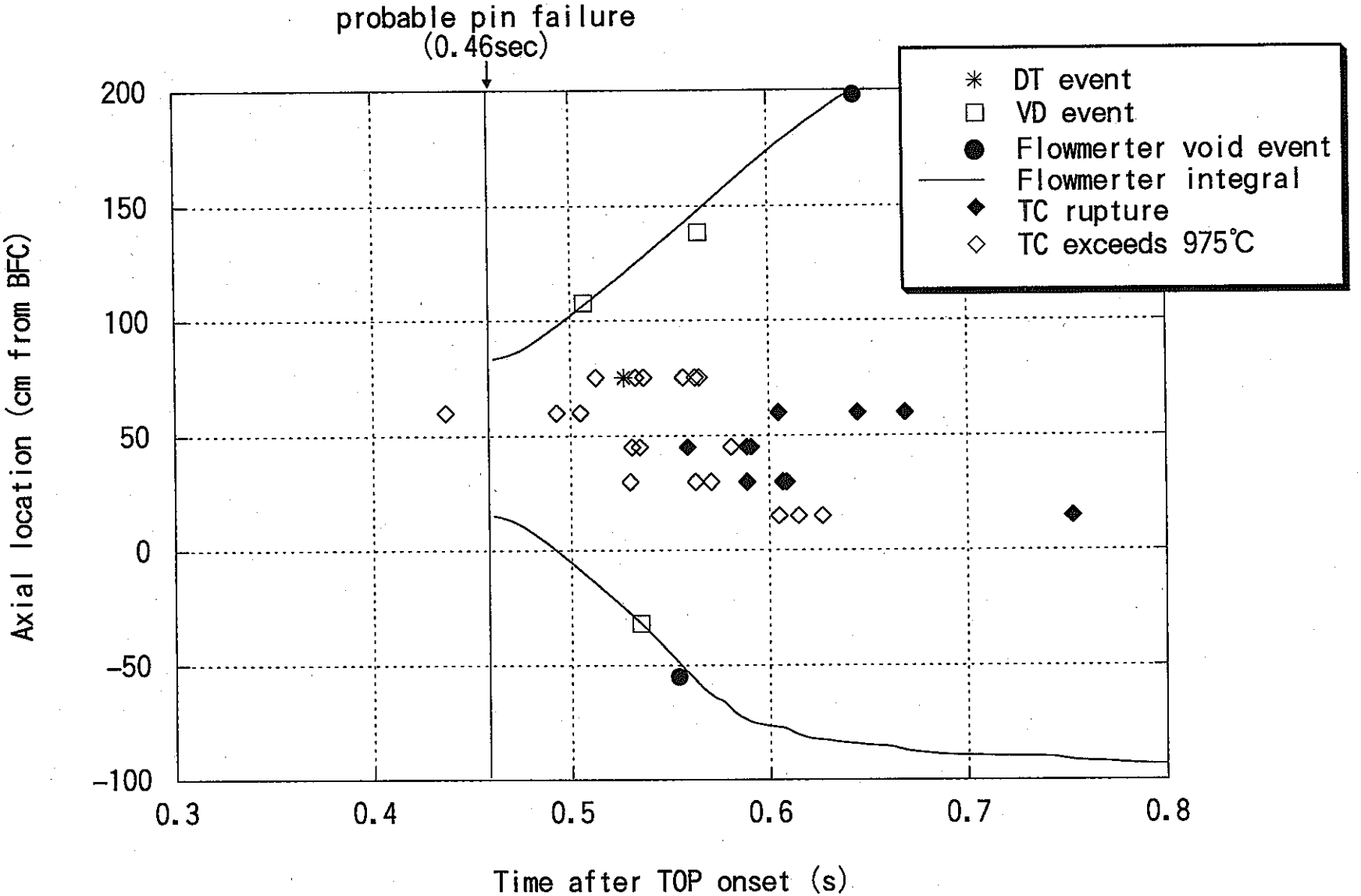

Figure 2.3 **Development of coolant-channel voiding**

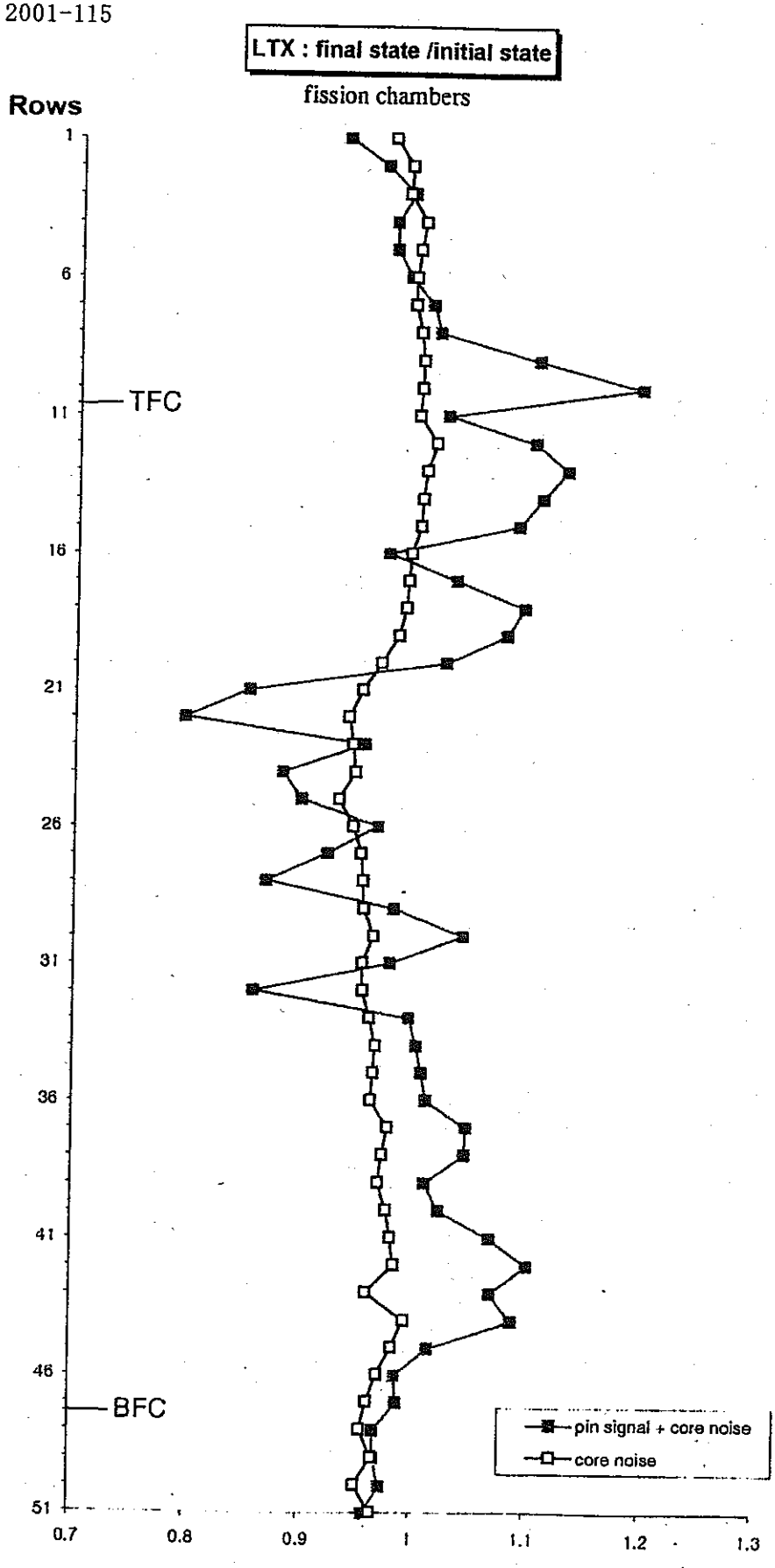

Fig. 2.4 Normalized hodoscope signal in the LTX test at the final state

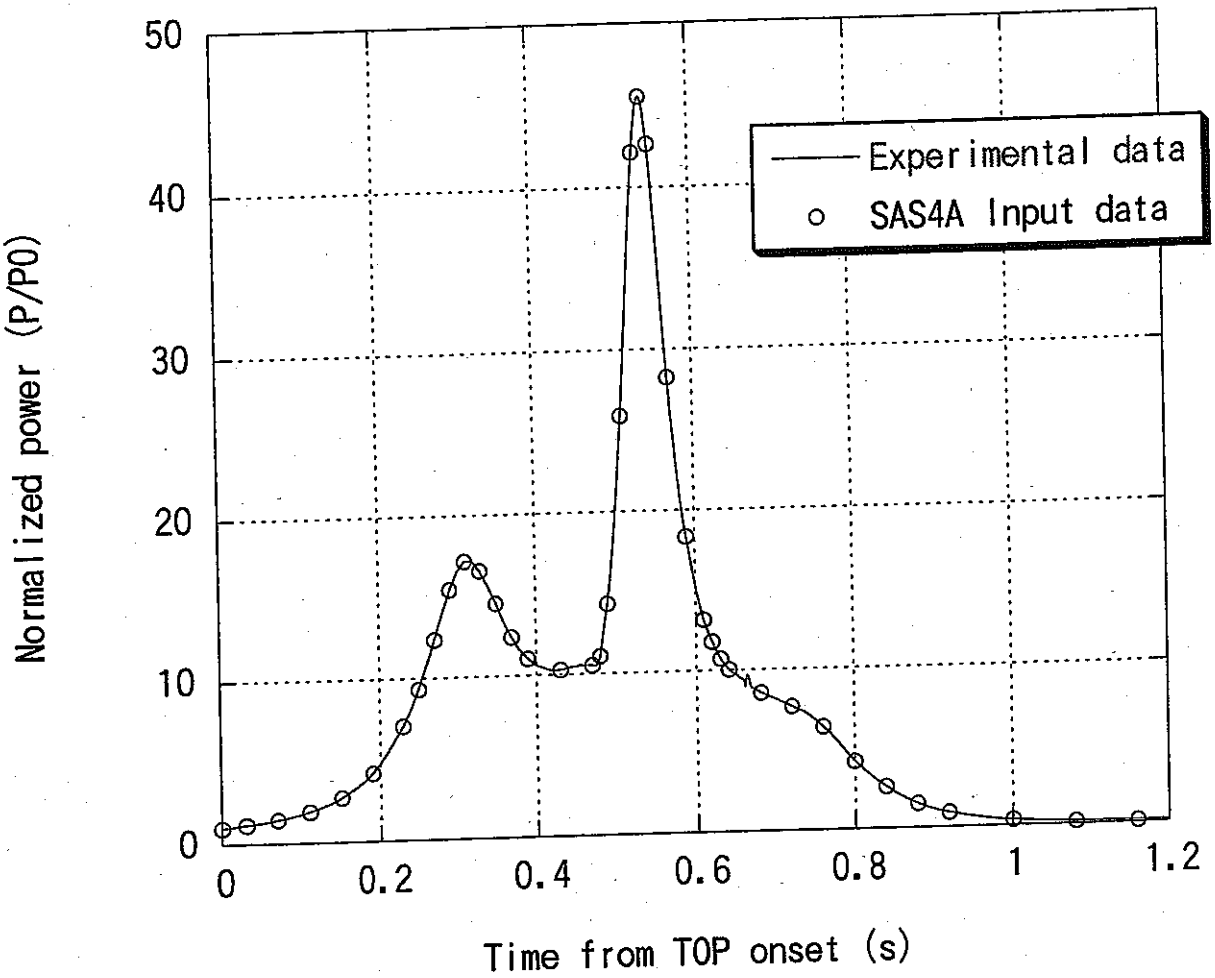

Figure 4.1 **Transient power history during TOP used in SAS4A calculation**

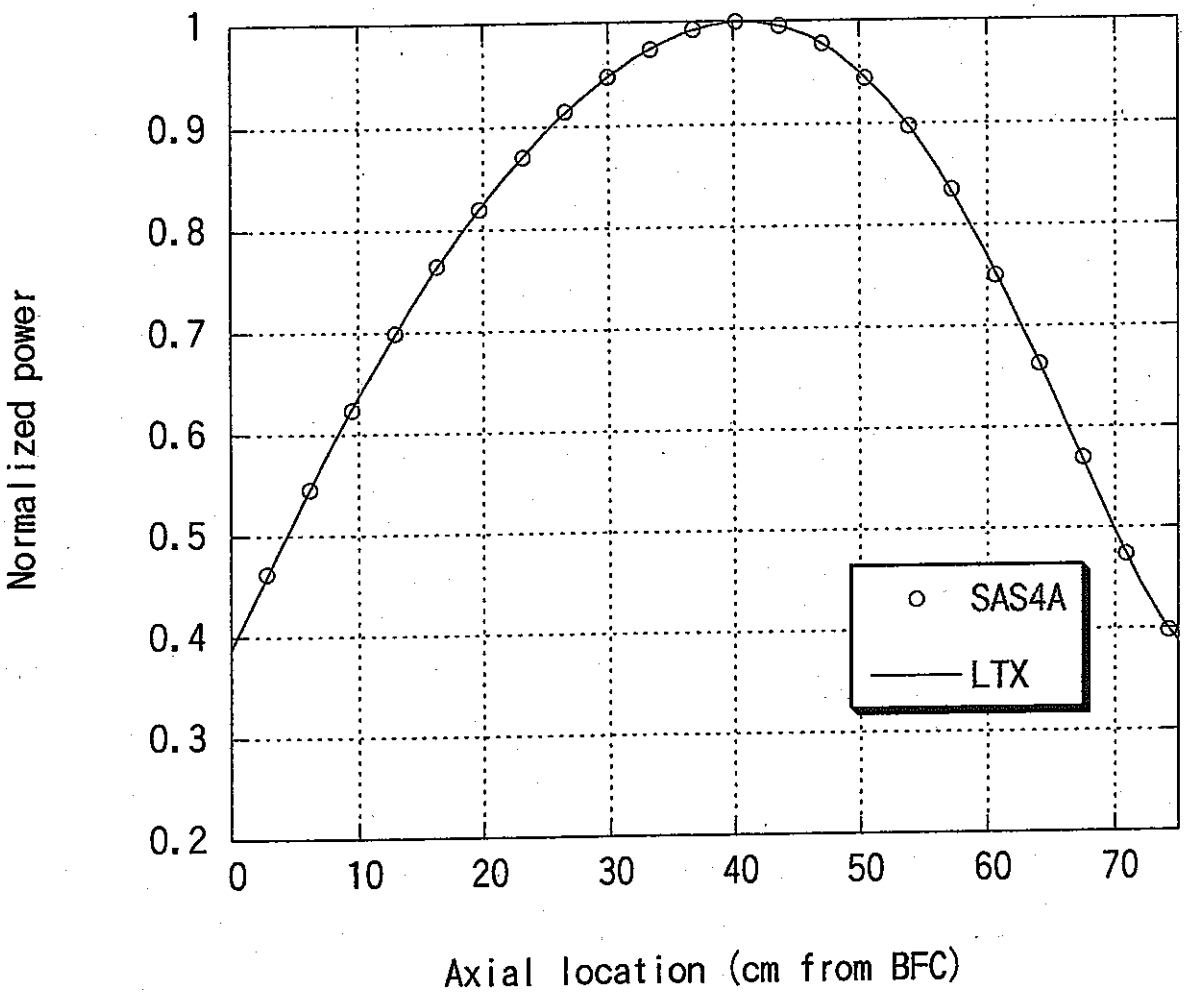

Figure 4.2 Axial power distributions used in SAS4A

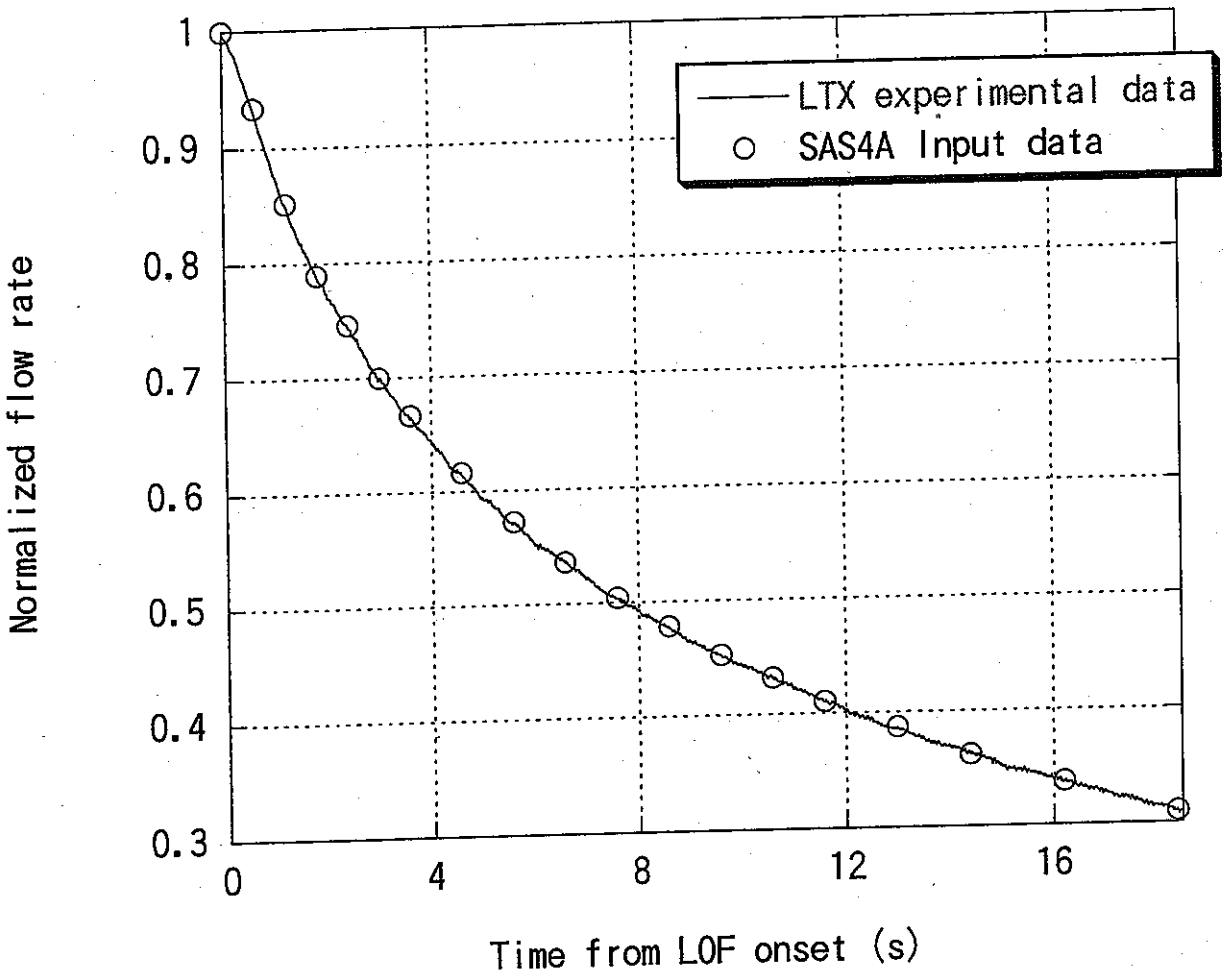

Figure 4.3 Flow rate history during LOF used in SAS4A

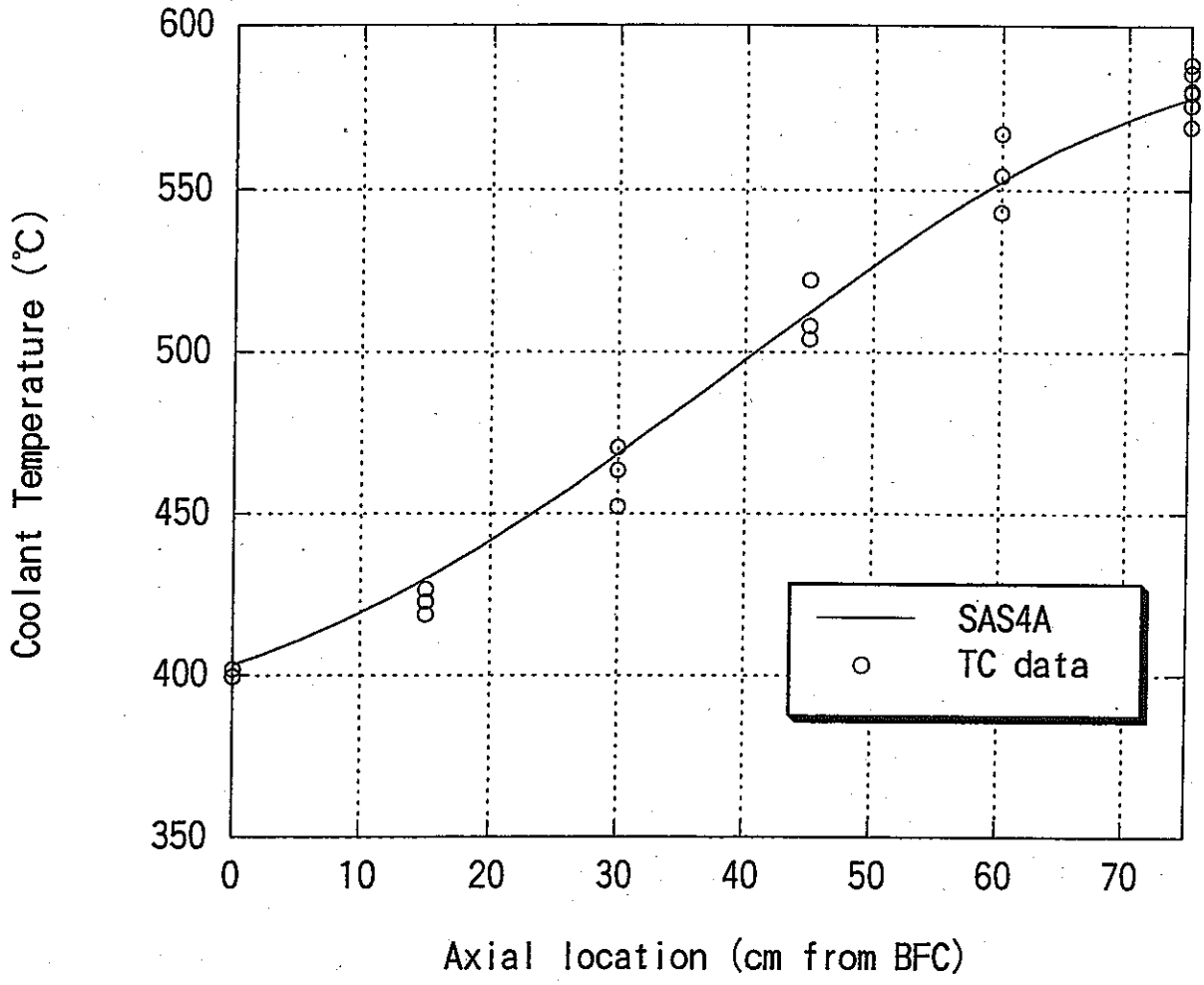

Figure 4.4 Comparison of coolant temperature profile at steady state

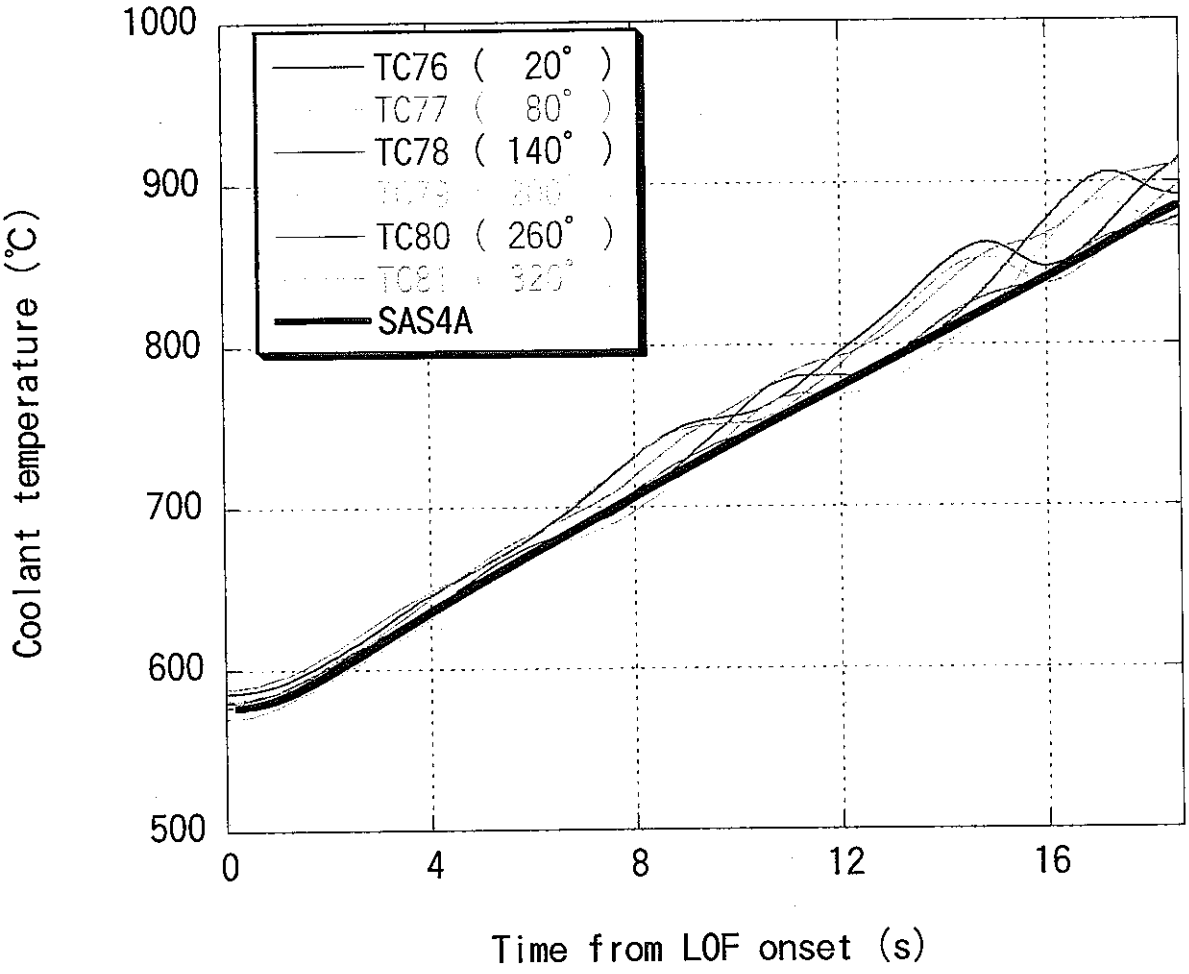

Figure 4.5 Comparison of coolant temperature history at TFC during LOF

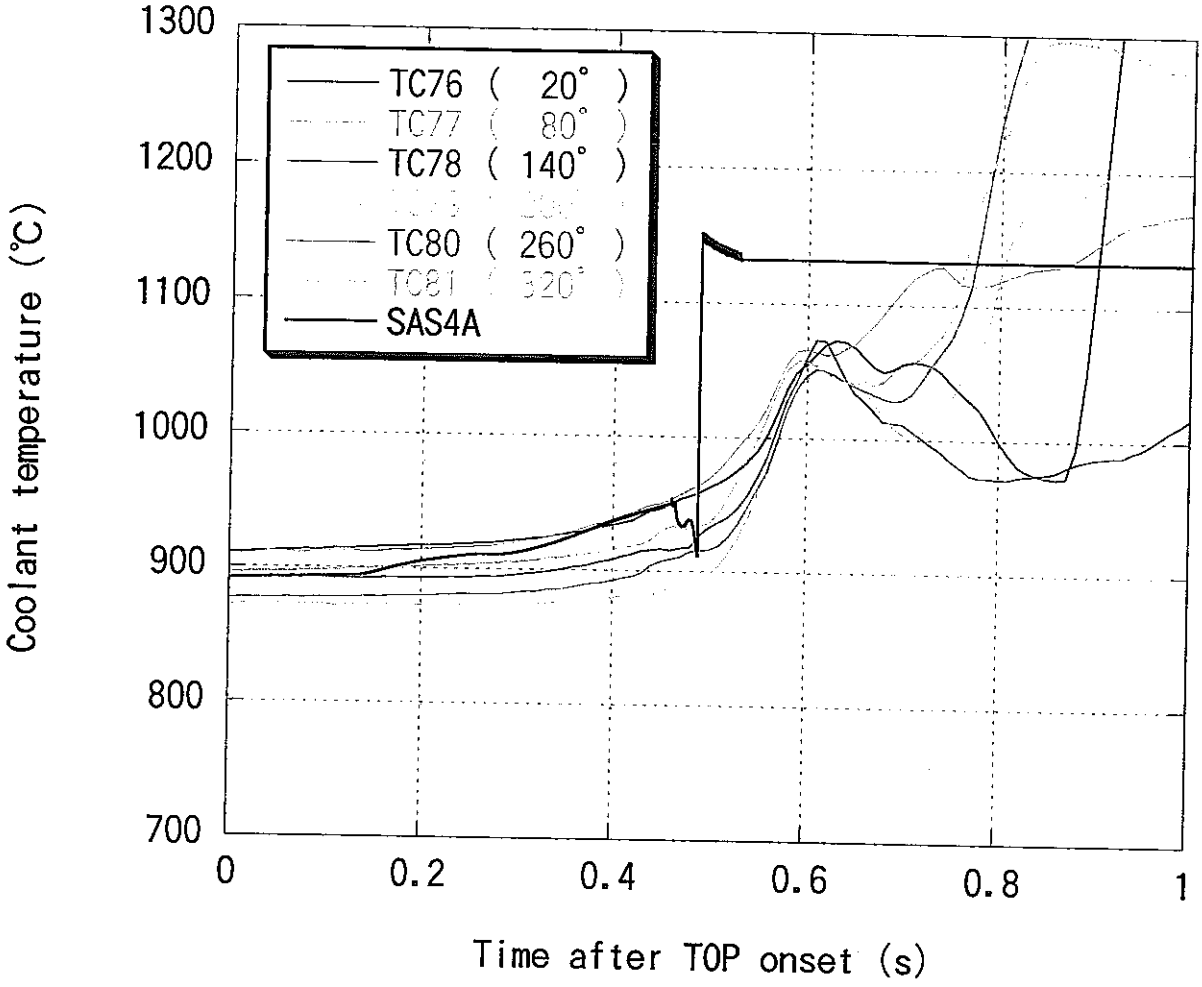

Figure 4.6 Coolant temperature history at TFC during TOP

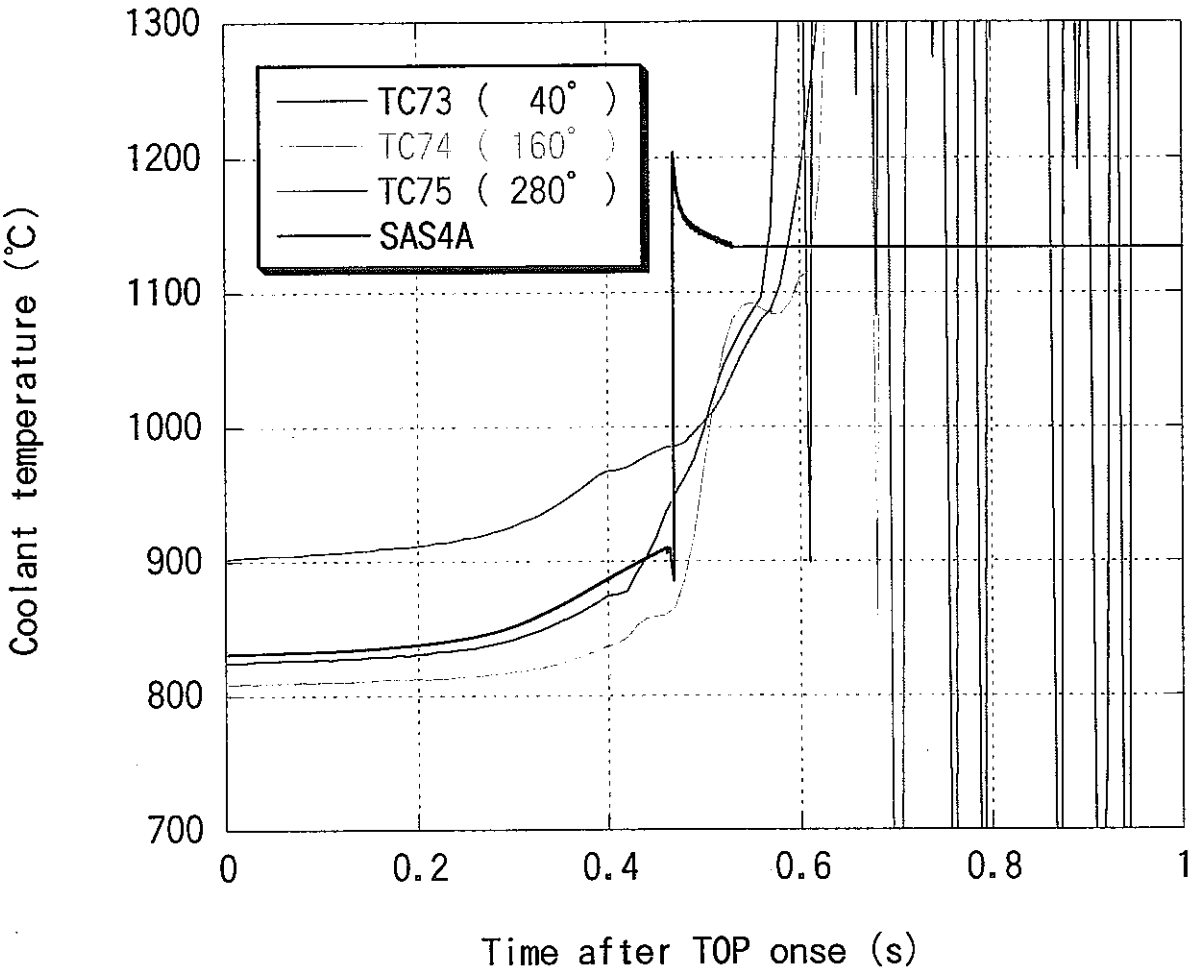

Figure 4.7 Coolant temperature history at 60cm from BFC during TOP

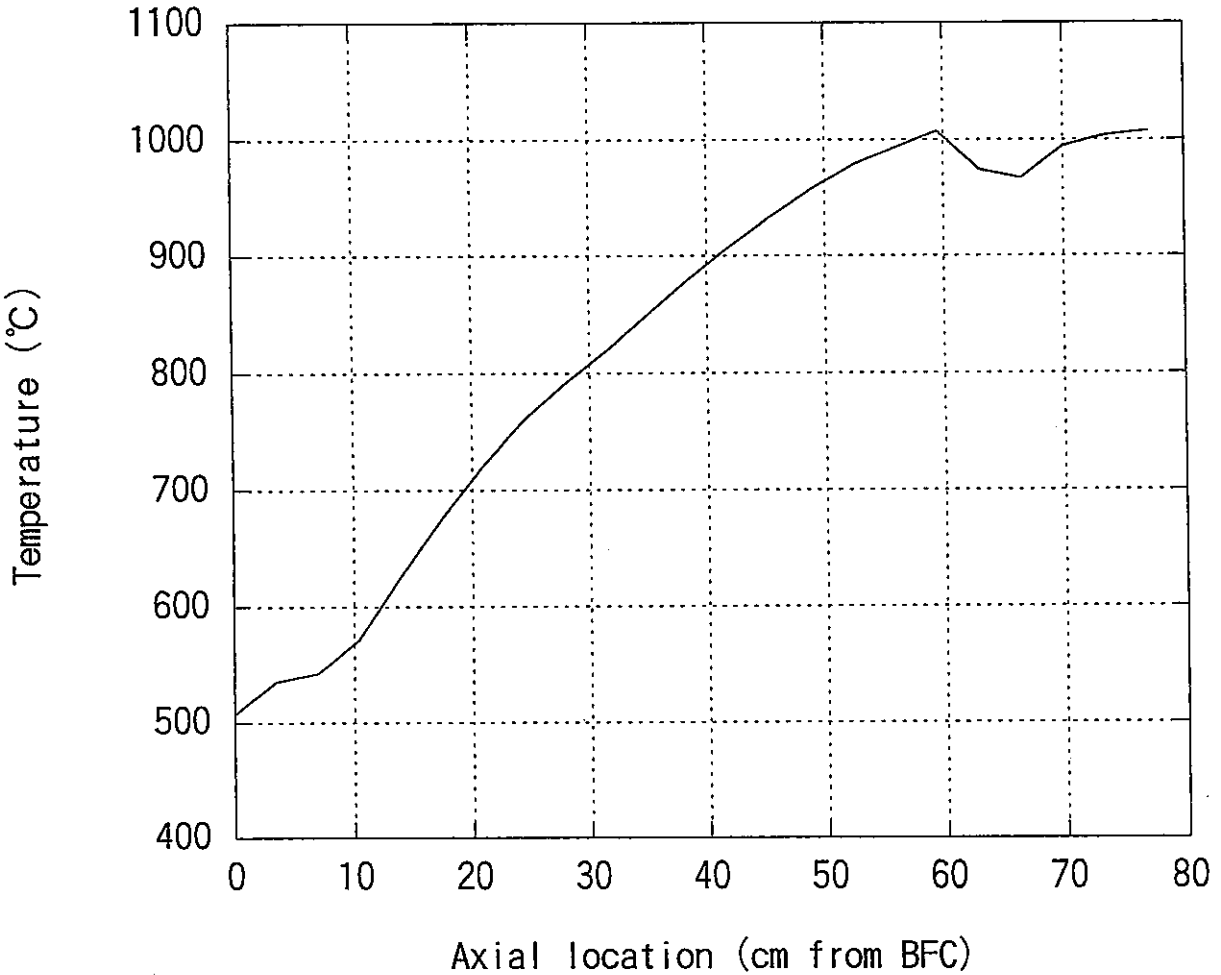

Figure 4.8 Axial clad midwall temperature calculated at 460 ms after TOP

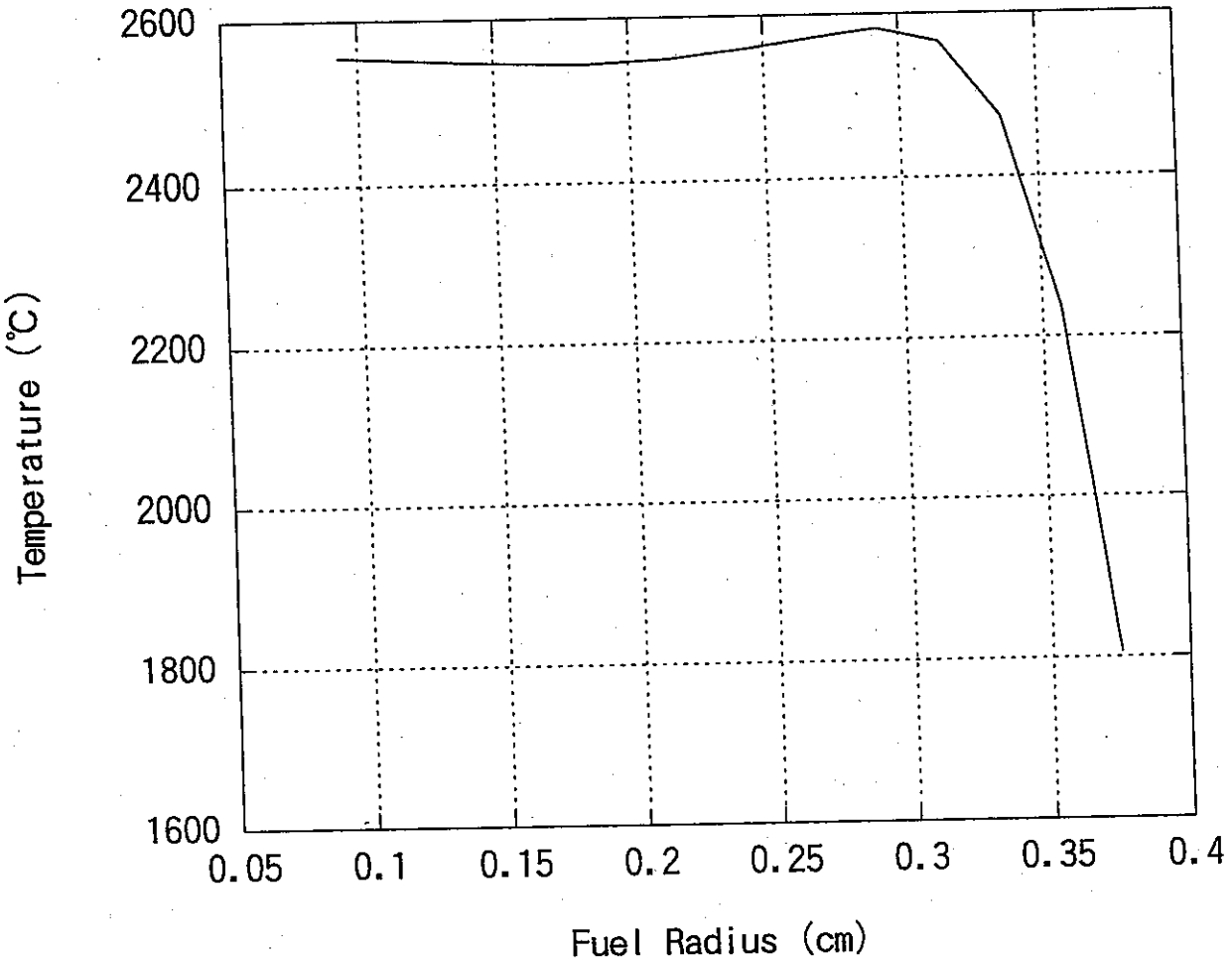

Figure 4.9 Radial fuel temperature distribution at PPN at 460 ms after TOP

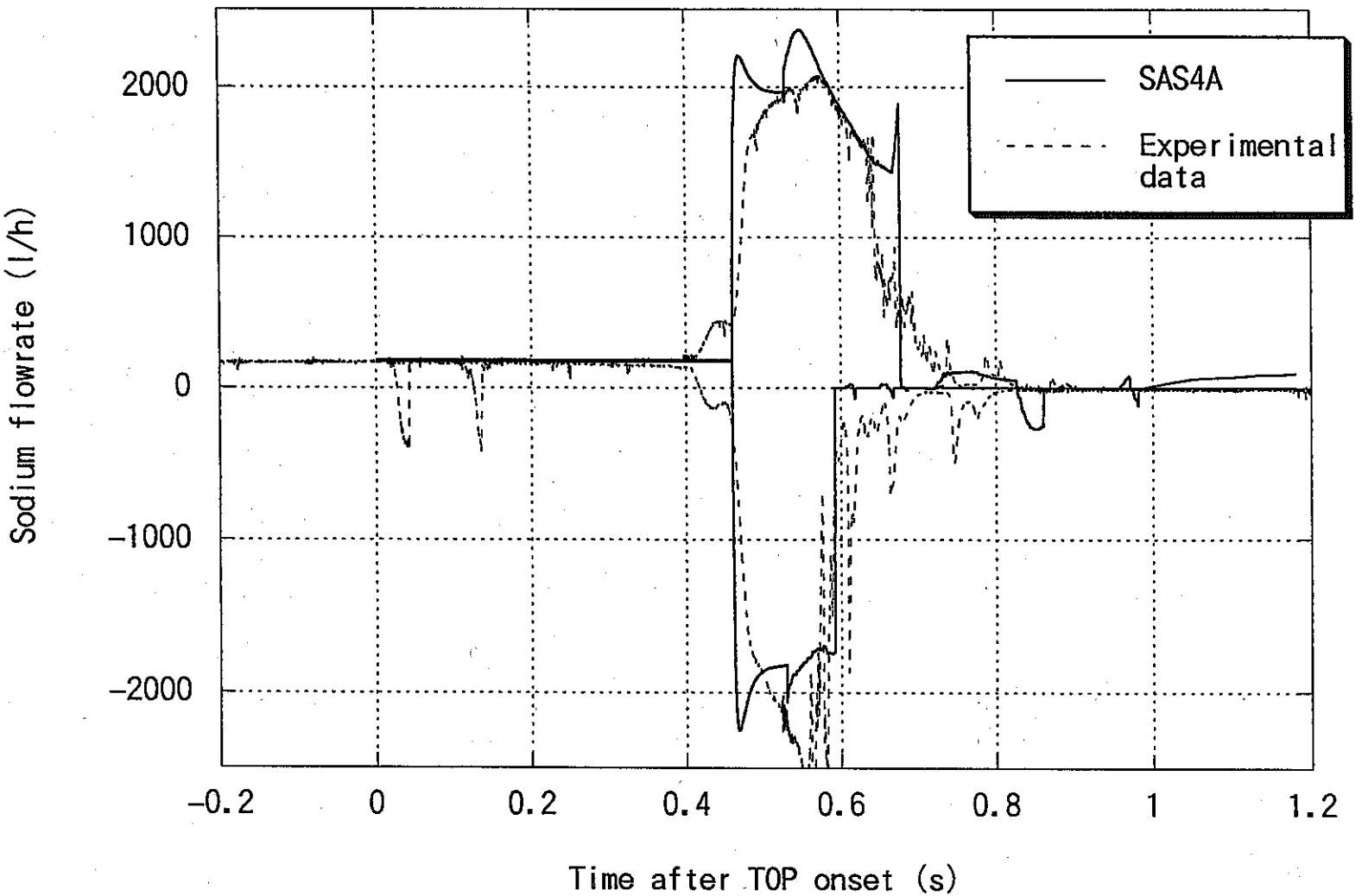

Figure 4.10 Coolant flow rates after the cladding failure

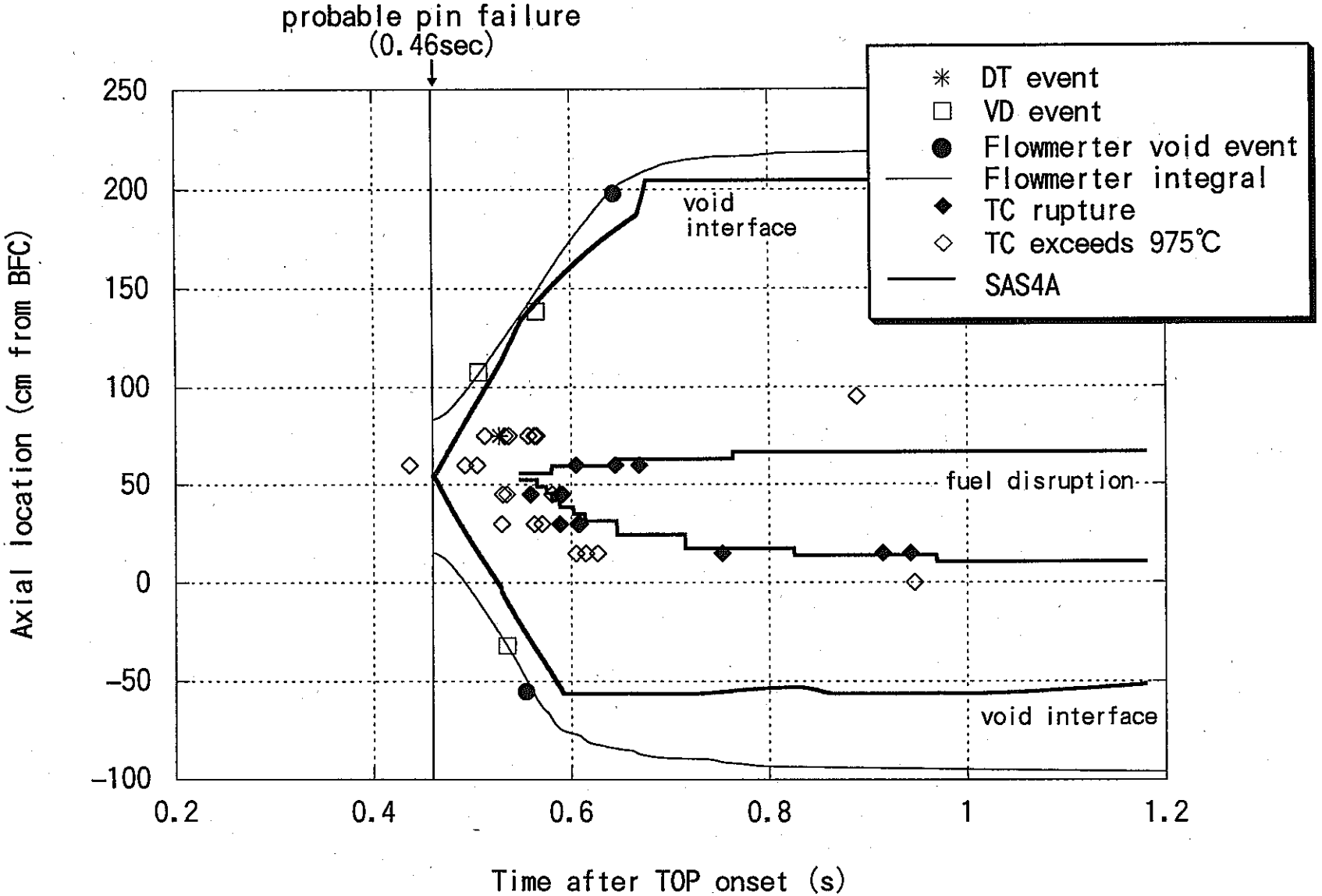

Figure 4.11 Coolant-channel voiding and fuel disruption fronts

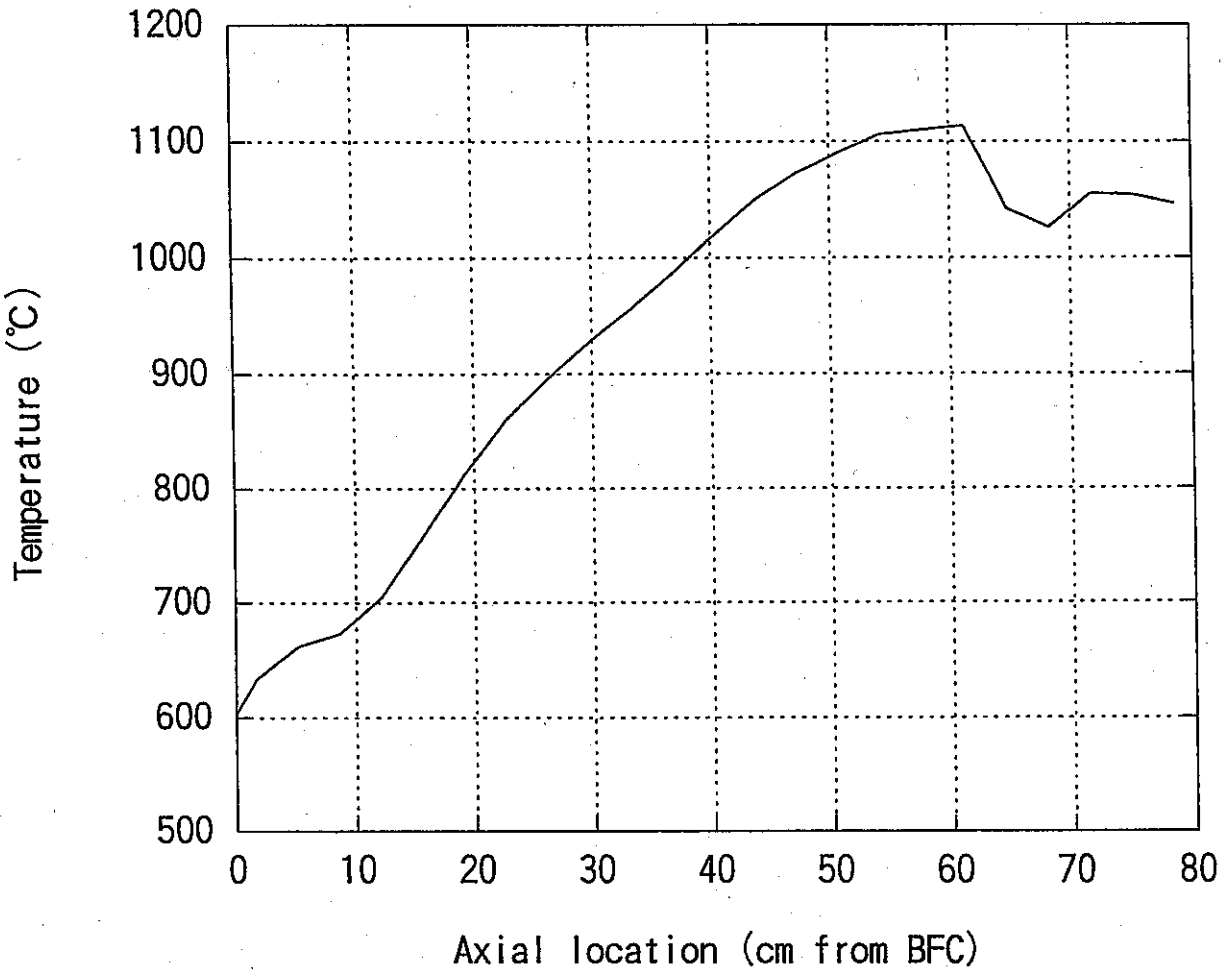

Figure 4.12 Axial distribution of clad midwall temperature at 530 ms after TOP

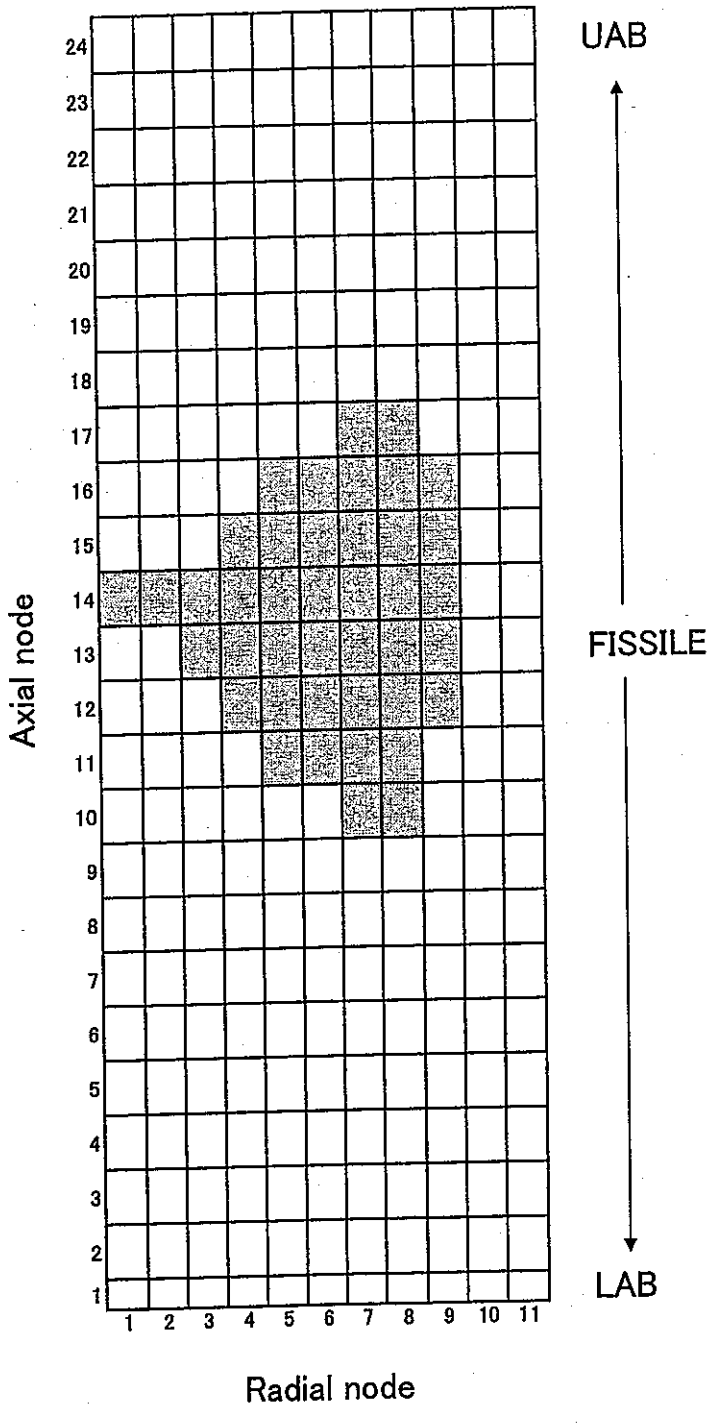

Fugure 4.13 Melting boundary at 530 ms after TOP

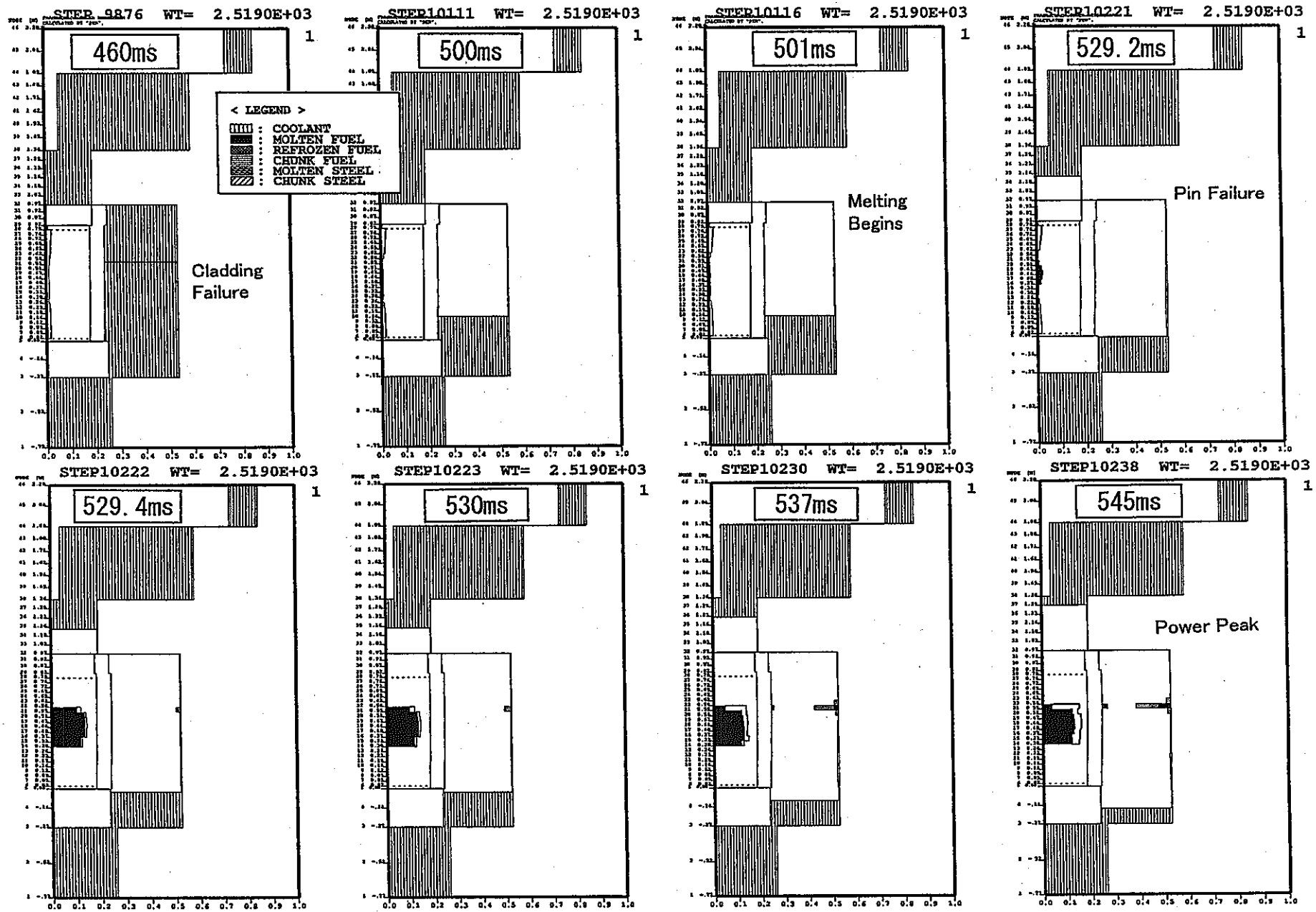

Figure 4.14 Volume fractions of the mixture before power peak during TOP

Figure 4.15 Volume fractions of the mixture after power peak during TOP

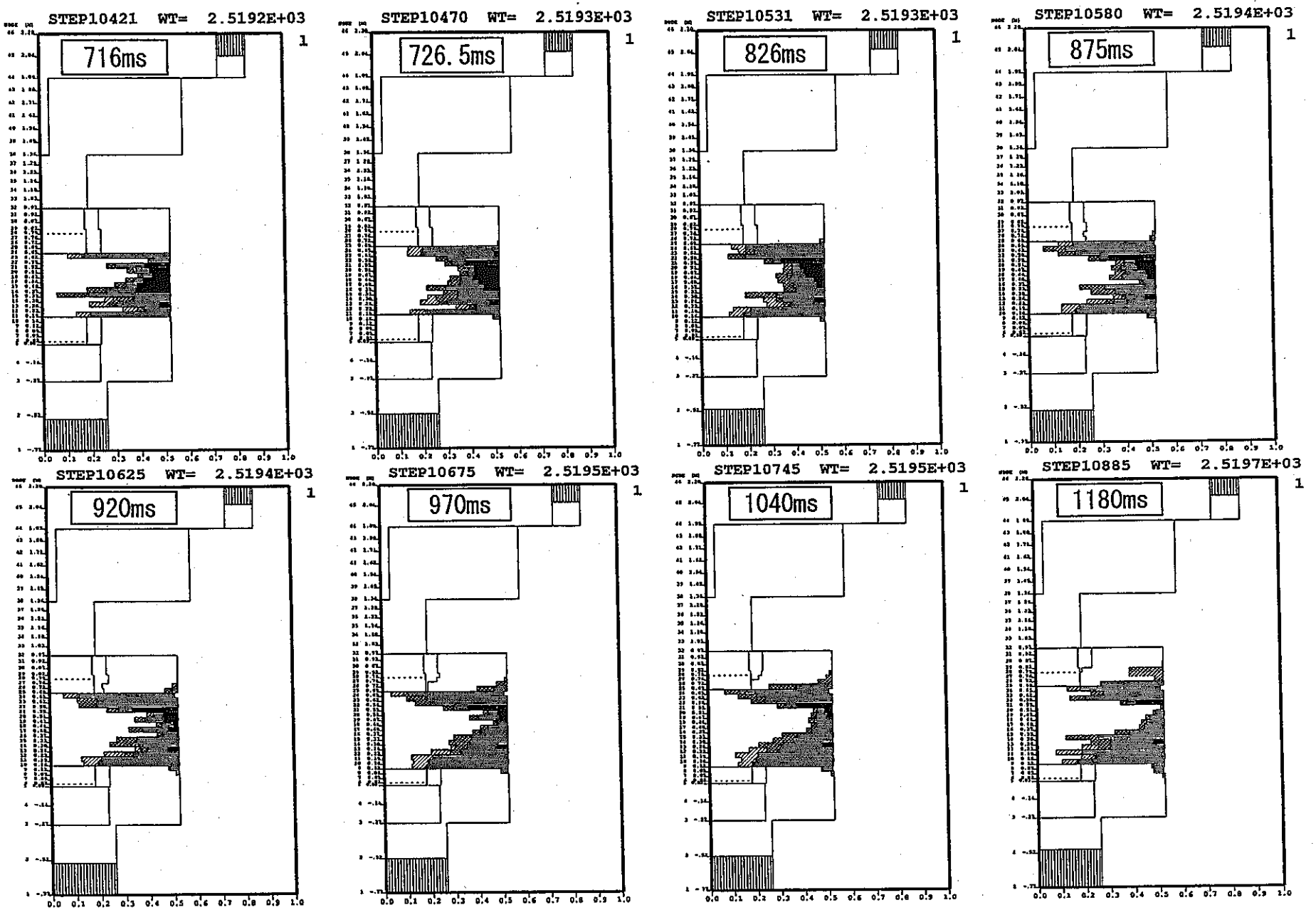

Figure 4.16 Volume fractions of the mixture after scram during TOP

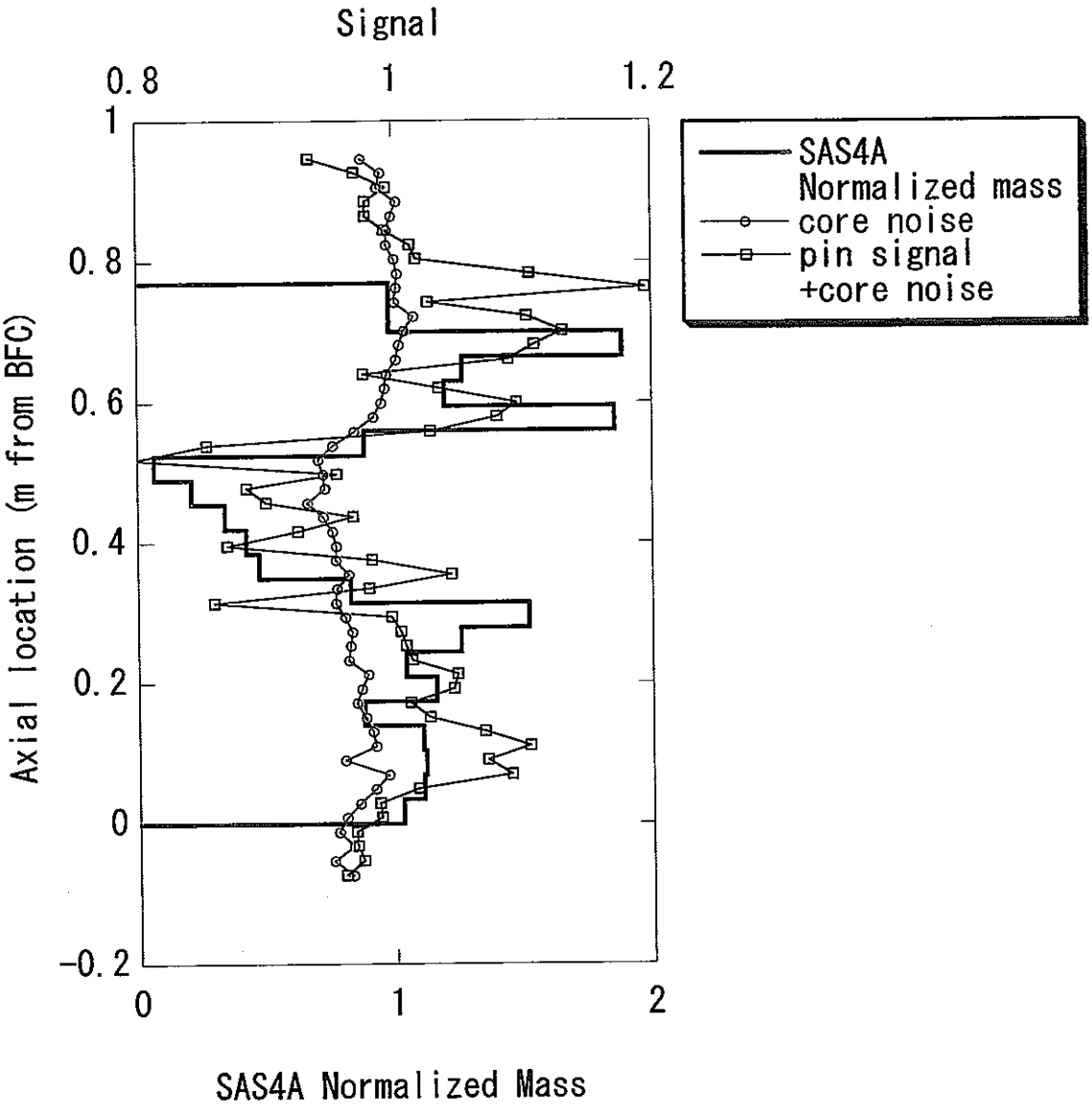

Figure 4.17 Comparison of final fuel configuration calculated by SAS4A to hodoscope data

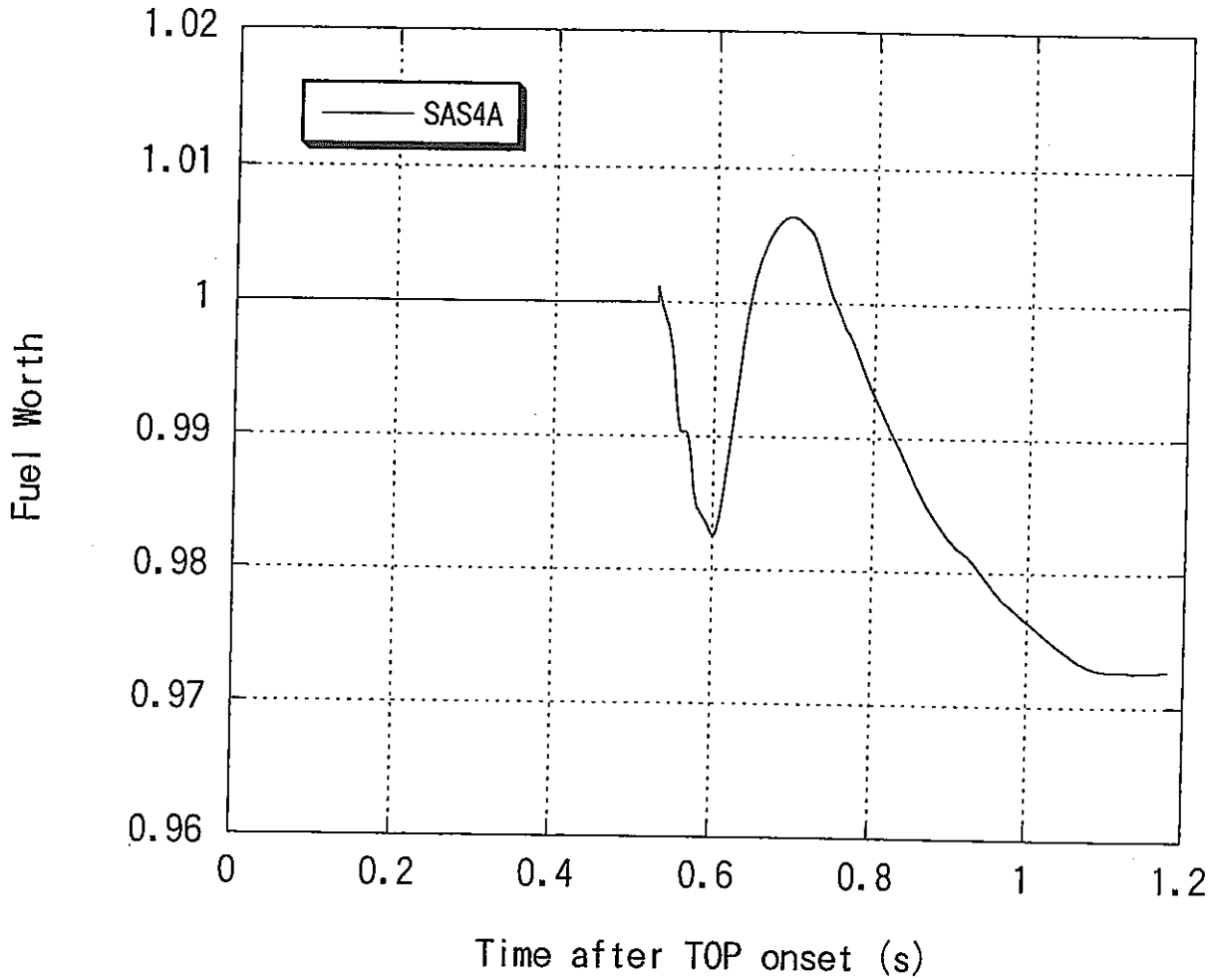

Figure 4.18 Relative fuel worth history during TOP